Differential cross sections, photon beam asymmetries, and spin density matrix elements of ω photoproduction off the proton at $E_\gamma = 1.3-2.4$ GeV

N. Muramatsu,[1] J. K. Ahn,[2] W. C. Chang,[3] J. Y. Chen,[4] M. L. Chu,[3] S. Daté,[5,6] T. Gogami,[7] H. Goto,[6] H. Hamano,[6] T. Hashimoto,[6] Q. H. He,[8] K. Hicks,[9] T. Hiraiwa,[10] Y. Honda,[1] T. Hotta,[6] H. Ikuno,[6] Y. Inoue,[1] T. Ishikawa,[1] I. Jaegle,[11] J. M. Jo,[2] Y. Kasamatsu,[6] H. Katsuragawa,[6] S. Kido,[1] Y. Kon,[6] S. Masumoto,[12] Y. Matsumura,[6] M. Miyabe,[1] K. Mizutani,[11] T. Nakamura,[13] T. Nakano,[6] T. Nam,[6] T. N. T. Ngan,[14] M. Niiyama,[15] Y. Nozawa,[16] Y. Ohashi,[5,6] H. Ohnishi,[1] T. Ohta,[16] K. Ozawa,[17] C. Rangacharyulu,[18] S. Y. Ryu,[6] Y. Sada,[1] T. Shibukawa,[12] H. Shimizu,[1] R. Shirai,[1] K. Shiraishi,[1] E. A. Strokovsky,[19,6] Y. Sugaya,[6] M. Sumihama,[13,6] S. Suzuki,[5] S. Tanaka,[6] Y. Taniguchi,[1] A. Tokiyasu,[1] N. Tomida,[6] Y. Tsuchikawa,[20] T. Ueda,[1] H. Yamazaki,[21] R. Yamazaki,[1] Y. Yanai,[6] T. Yorita,[6] C. Yoshida,[1] and M. Yosoi[6]
(LEPS2/BGOegg Collaboration)

[1]*Research Center for Electron Photon Science, Tohoku University, Sendai, Miyagi 982-0826, Japan*
[2]*Department of Physics, Korea University, Seoul 02841, Republic of Korea*
[3]*Institute of Physics, Academia Sinica, Taipei 11529, Taiwan*
[4]*National Synchrotron Radiation Research Center, Hsinchu 30076, Taiwan*
[5]*Japan Synchrotron Radiation Research Institute (SPring-8), Sayo, Hyogo 679-5198, Japan*
[6]*Research Center for Nuclear Physics, Osaka University, Ibaraki, Osaka 567-0047, Japan*
[7]*Department of Physics, Kyoto University, Kyoto 606-8502, Japan*
[8]*Department of Nuclear Science & Engineering, College of Material Science and Technology, Nanjing University of Aeronautics and Astronautics, Nanjing 210016, China*
[9]*Department of Physics and Astronomy, Ohio University, Athens, Ohio 45701, USA*
[10]*RIKEN SPring-8 Center, Sayo, Hyogo 679-5148, Japan*
[11]*Thomas Jefferson National Accelerator Facility, Newport News, Virginia 23606, USA*
[12]*Department of Physics, University of Tokyo, Tokyo 113-0033, Japan*
[13]*Department of Education, Gifu University, Gifu 501-1193, Japan*
[14]*Nuclear Physics Department, University of Science, Vietnam National University, Ho Chi Minh City, Vietnam*
[15]*Department of Physics, Kyoto Sangyo University, Kyoto 603-8555, Japan*
[16]*Department of Radiology, The University of Tokyo Hospital, Tokyo 113-8655, Japan*
[17]*Institute of Particle and Nuclear Studies, High Energy Accelerator Research Organization (KEK), Tsukuba, Ibaraki 305-0801, Japan*
[18]*Department of Physics and Engineering Physics, University of Saskatchewan, Saskatoon, Saskatchewan, Canada S7N 5E2*
[19]*Laboratory of High Energy Physics, Joint Institute for Nuclear Research, Dubna, Moscow Region 142281, Russia*
[20]*J-PARC Center, Japan Atomic Energy Agency, Tokai, Ibaraki 319-1195, Japan*
[21]*Radiation Science Center, High Energy Accelerator Research Organization (KEK), Tokai, Ibaraki 319-1195, Japan*

(Received 27 March 2020; accepted 2 July 2020; published 3 August 2020)

For the reaction $\gamma p \to \omega p$, differential cross sections, photon beam asymmetries, and spin density matrix elements have been measured in the BGOegg experiment at the SPring-8 LEPS2 beamline by using a large acceptance electromagnetic calorimeter. A 1.3–2.4 GeV photon beam with high linear polarization has enabled a precision measurement of photon beam asymmetries Σ and polarized spin density matrix elements ρ^1_{1-1} over a wide angular range, especially above the total energy of about 2 GeV for the first time. The measured ρ^1_{1-1} indicates the dominance of s-channel resonances even at higher energies. The Σ values at backward angles are not reproduced by the existing partial-wave analysis in the highest-energy region, providing new constraints to the contribution of nucleon resonances with high spins.

DOI: 10.1103/PhysRevC.102.025201

I. INTRODUCTION

The internal structure of nucleons is a longstanding issue to understand the dynamics of quarks and gluons in the confinement regime. The mass spectra of nucleon resonances are expected to provide information on the composition of hadrons [1]. While the low-lying states are successfully explained by constituent quark models and lattice QCD calculations, highly excited states are not well reproduced by theoretical attempts yet, indicating mass deviations and missing resonances. It is definitely desired to establish such high-mass resonances from the experimental side. These efforts will enhance progress in the understanding of interquark forces, diquark correlations, and so on [2].

Nonstrange nucleon resonances have been extensively examined through various experiments of πN scattering and

π electro- and photoproduction [3]. However, the discrimination between different isospin states, namely nucleon and Δ resonances (N^*s and Δ^*s, respectively), is difficult for excited states in the system of a pion ($I = 1$) and a nucleon ($I = 1/2$). In contrast, photoproduction of the ω meson, which has an isoscalar nature, provides a good opportunity to probe $I = 1/2$ N^*s only. In addition, the natural width of the ω meson is narrow, so that the reaction process of $\gamma p \to \omega p$ can be unambiguously identified with a kinematic fit by using a proton target.

Therefore, ω-photoproduction data have been collected with a liquid hydrogen target in the BGOegg experiment at the SPring-8 LEPS2 beamline. We have measured differential cross sections and photon beam asymmetries by using a high-intensity photon beam with linear polarization. Simultaneous measurement of these observables offers a way to differentiate individual N^* contributions, because many states with high spins and wide widths overlap with each other in the mass range above the so-called "third resonance" region [4]. We have also obtained spin density matrix elements, which express the decay pattern of a vector meson like ω. For N^* resonances, their spin information can be examined with reaction mechanisms through the unpolarized elements ρ^0_{00} and ρ^0_{1-1} as well as the polarized element ρ^1_{1-1}.

In the following part of this article, the experimental setup and analysis procedure are described in Secs. II and III, respectively. Then, the results for differential cross sections, photon beam asymmetries, and spin density matrix elements are shown in Sec. IV, followed by discussions in Sec. V. Finally, Sec. VI presents a summary.

II. EXPERIMENT

This section gives a brief explanation of the experimental setup. More details are described in Ref. [5].

The experiment to study ω photoproduction was conducted by using a large solid angle electromagnetic calorimeter, called BGOegg, and associated detectors for charged particles. The BGOegg calorimeter consists of 1320 bismuth germanate (BGO) crystals, surrounding a target in the polar angle range from 24° to 144°. Neighboring BGO crystals with energy deposits were connected as a cluster around the highest-energy crystal. The energy resolution for γ's is 1.3% at 1 GeV [6], which is the world's best in a sub-GeV energy region. Inside the BGOegg calorimeter, 30 slats of 453-mm-long inner plastic scintillators (IPS) were installed side by side in a ring-shape around the photon beam axis. The charge of a particle hitting the BGOegg calorimeter was determined by examining the existence of an IPS hit in the direction of the reconstructed cluster.

The forward acceptance hole of the BGOegg calorimeter was covered by a planar drift chamber (DC) to detect charged particles. The DC is made in a hexagonal shape with six drift planes, whose inscribed circle has a diameter of 1280 mm. There are three directions for anode wires with an azimuthal angle difference of 60°. The direction of charged particles coming from a 1.6-m-upstream target was measured by fitting a straight line to four or more DC hits and the target center.

A liquid hydrogen (LH_2) target was installed at the center of the BGOegg calorimeter. Liquefied hydrogen was filled inside a 54-mm-length polyimide film cell, which was connected to a refrigerator system located about 0.8 m upstream through a long cylindrical copper pipe. This target was exposed to a photon beam produced by laser Compton scattering with the maximum energy of 2.4 GeV [7]. The distance from the Compton scattering point to the target reached 125 m. Although most of this space was occupied by a long vacuum pipe for photon beam transportation, the transmission rate to the target was 0.772 due to end-window materials, an x-ray shield, and short air spaces. The contamination of e^+e^- conversions in the photon beam was removed by using a 3-mm-thick plastic scintillator (UpVeto counter), located just upstream of the target refrigerator system. The photon beam incident on the LH_2 target was linearly polarized with high degrees by taking over the laser polarization of approximately 98%.

The energies of beam photons were measured event by event with a tagging detector (tagger), which detected recoil electrons from laser Compton scattering. The tagger was placed at the downstream exit of a SPring-8 bending magnet to analyze the momenta of recoil electrons with their hit positions at two walls of plastic scintillating fibers. The photon beam energy can be tagged in the range above 1.3 GeV, which is limited by the tagger acceptance. The tagger also has 8-mm-wide plastic scintillators for triggers. Only one recoil electron track was accepted at the timing of BGOegg calorimeter hits, after confirming a good reconstruction pattern with two-wall fiber and trigger scintillator hits. The flux of the photon beam and its integrated number during an experimental period were derived by counting hits at the tagger trigger scintillators. The total number of photons reached 3.586×10^{12} in the present analysis after correcting for inefficiencies due to electron filling patterns at SPring-8 [8].

III. DATA ANALYSIS

A. Event selection

Event selection conditions are basically the same as those in the published article on π^0 photoproduction [5], except for identifying ω mesons in the $\pi^0\gamma$-decay mode, whose branching fraction is 0.0840 ± 0.0022 [9]. Thus, events with three neutral clusters were selected as signal candidates, if the time differences of these clusters were less than 10 ns. Clusters whose central crystal was found at the most-forward or most-backward edge of the BGOegg calorimeter were not used, to avoid insufficient measurement of cluster energies. The minimum energy of individual clusters was required to be 30 MeV to remove accidental hits. The shape of clusters provides additional information about the type of calorimeter hits. There were unusually shaped clusters due to unrelated reaction products from upstream materials. Events having such a cluster were omitted when the effective cluster size [5] was larger than 20 mm. Small energy-leak clusters, corresponding to the split-offs of an electromagnetic shower, were identified by their characteristics such as a shorter distance to a main cluster, a smaller energy, a smaller number of cluster

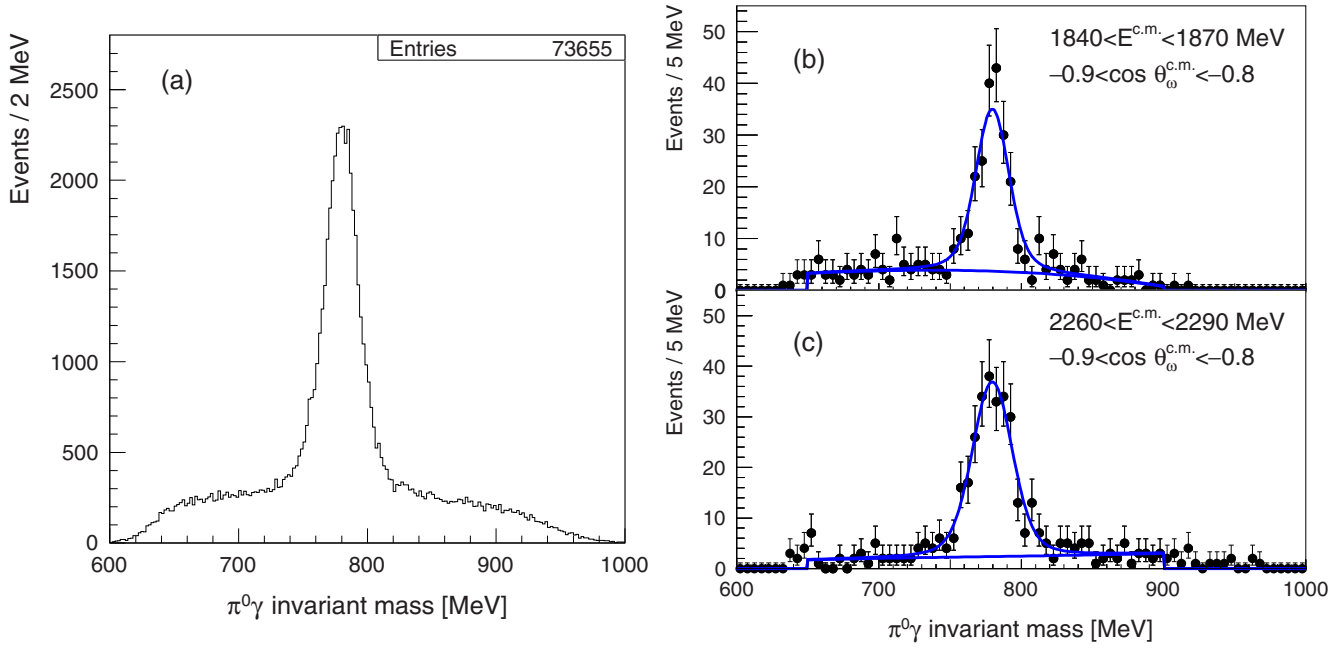

FIG. 1. Distributions of $\pi^0\gamma$ invariant mass. Panel (a) shows the distribution for the whole selected sample, while panels (b) and (c) are examples of fits with signal and background functions in two kinematical bins, whose conditions are displayed in each panel.

member crystals, and an unusual shape with a larger effective size. These conditions were determined by a Monte Carlo (MC) simulation, whose source package was developed for the BGOegg experiment based on GEANT4 [10]. The identified leak clusters were combined with the main cluster to sum up their energies. As a result, the number of signal events increased by 13.5% even after requiring a condition that there be no more than three neutral clusters. This rate of increase is consistent with the MC simulation result.

A proton in the final state was detected at either the BGOegg calorimeter or the DC. Only the proton-emission angle was measured (no particle identification). Because the momentum of a backward-going proton was low due to the large ω mass, a time-of-flight effect was taken into account for the time windows of the BGOegg-calorimeter and IPS hits. The IPS timing and energy deposit, which were read out only from the upstream ends, were calibrated depending on the polar angle of each charged cluster. At the DC, the χ^2 probability of a straight-line fit was required to be larger than 0.01. The left-right ambiguity of DC hits and the removal of outlier hits with large residuals were judged based on the χ^2 probability. Finally, the total number of charged tracks was limited to one, except for special treatments for e^+e^- conversions at the target and proton interactions at BGO crystals near the DC [5].

After measuring all the final-state particles, a four-constraint (4C) kinematic fit was performed by assuming the reaction $\gamma p \to \omega p \to \pi^0\gamma p \to \gamma\gamma\gamma p$. We treated the following 13 quantities as measured variables: the photon beam energy, the z-position of a reaction vertex, the energies of three γ's, and the polar and azimuthal angles of these γ's and a proton. Conservation of the four-momentum between the initial and final states was required by using the above variables with resolution inputs and an unmeasured variable for the magnitude of the proton momentum. The invariant mass of two γ's was constrained to the nominal value of the π^0 mass, while the best combination of the two γ's was chosen from three possibilities based on a χ^2 probability of the kinematic fit. The $\pi^0\gamma$ invariant mass was not constrained to the ω mass because of its natural width. The final sample was selected by requiring the χ^2 probability, whose distribution was flat for signals, to be greater than 0.02.

B. Signal yield extraction

About 74 000 events remain in the final sample. As shown in Fig. 1(a), the $\pi^0\gamma$-invariant-mass distribution includes a broad background component under a signal peak. Contamination of the background component happens because of no constraint on the ω mass in the kinematic fit. It has been confirmed that this background component is dominated by the reaction $\gamma p \to \pi^0\pi^0 p$ with one γ escaping into the forward acceptance hole of the BGOegg calorimeter.

The number of ω-photoproduction signals was obtained by fitting signal and background functions to the $\pi^0\gamma$-invariant-mass spectra in individual kinematical bins of the center-of-mass energy and the ω polar angle, which were used in the derivation of differential cross sections, photon beam asymmetries, and spin density matrix elements. The signal function was represented by a Voigt function, where the width of a Breit-Wigner component was fixed to the natural width of the ω-meson mass (8.49 MeV/c^2). The convoluted mass resolution was also predetermined by smoothening the resolutions obtained from Voigt function fits with free resolution parameters in all the kinematical bins. The predetermined function provides a mass resolution of 9–12 MeV/c^2 depending on the center-of-mass energy. Background template spectra were prepared in individual kinematical bins by fitting third-order

polynomial functions to the $\pi^0\gamma$-invariant-mass distributions generated by MC simulations of the reaction $\gamma p \to \pi^0\pi^0 p$. Here, several processes including the production of nonresonant $\pi^0\pi^0 p$, $\pi^0\Delta^+$, $\pi^0 N(1520)^+$, etc., were simulated, and the generated samples were added after scaling their relative contributions by a separate analysis of the real data with four-γ detection.

Fittings of the signal and background functions were performed by using a maximum likelihood method. Figures 1(b) and 1(c) show examples of the fit results in two kinematical bins. In the fits, means and vertical scales were varied for the signal functions, while only scales were adjusted for the background template spectra. The ω-photoproduction yields were evaluated from the scales of fitted signal functions in individual kinematical bins. A sum of the extracted signal yields reaches about 37 000 events.

C. Efficiency estimation

The geometrical acceptance and the efficiencies due to the detector responses and the physical processes in materials were evaluated by the realistic MC simulation with the BGOegg experimental setup. The $\gamma p \to \omega p \to \pi^0\gamma p$ events were generated with the energy dependence proportional to the photon beam energy spectrum of laser Compton scattering. The angular distribution of final-state particles were isotropic at first. The same event selection conditions as those in the real data analysis were applied to the generated sample for the acceptance measurement.

Acceptance factors measured by using the above MC sample must be corrected, reflecting true angular and energy distributions inside the individual kinematical bins. The realistic distributions were taken into account in the simulation sample by adopting the measured differential cross sections and the ω-decay angular distributions described by experimental values of the spin density matrix element ρ^0_{00}. New acceptance factors with the updated MC sample were used at the next step of cross-section and decay-asymmetry measurements. This procedure was iterated until the acceptance factors became stable within approximately 1%. The obtained acceptance factors are typically around 50% for the ω detection at backward angles, and they decrease at forward angles. The ω mesons are reasonably detectable up to $\cos\theta_\omega^{\mathrm{c.m.}} \approx 0.8$.

The efficiencies that cannot be simulated by the MC package were separately estimated from the real data. Tagger detection and reconstruction efficiencies, proton detection efficiencies at the BGOegg calorimeter and the DC, and the survival rate after overvetoing extra charged particles due to the e^+e^- conversions of beam photons at the target were individually evaluated by using clean samples of photoproduction reactions with tight event selection, as described in Ref. [5]. The e^+e^- conversion of γ's from the ω decay occurs at the target and detector materials, resulting in a 5−13% loss depending on the ω polar angle when requiring no IPS hits for γ clusters. This effect was simulated by the MC package, but the estimated efficiencies were further corrected based on the measurement using real data to quantify imperfect inclusion of materials in the simulation. The data acquisition efficiency of accepted to triggered events was also evaluated to be about 95%. The trigger condition was defined by the coincidence of a tagger hit and two or more hits in 1320 BGO crystals.

IV. RESULTS

A. Differential cross section

Differential cross sections were measured at the total energies ($E^{\mathrm{c.m.}}$) of 1810–2320 MeV with a bin size of 30 MeV. The range of ω-emission angles in the center-of-mass frame was divided into 0.1-step bins in $\cos\theta_\omega^{\mathrm{c.m.}}$. Regions of insensitive acceptance, corresponding to the most-forward ω production, were omitted from the measurement. In the individual kinematical bins, the signal yields obtained in Sec. III B were corrected by the acceptance factors and efficiencies in Sec. III C as well as the branching fractions of the decays $\omega \to \pi^0\gamma$ and $\pi^0 \to \gamma\gamma$ [9]. Then, the corrected yields of ω photoproduction were divided by the luminosities, which were given by multiplying the numbers of protons in the LH_2 target and photons in the incident beam.

The number of beam photons measured by the tagger was contaminated with electromagnetic shower hits, which originated from low-energy recoil electrons colliding with the walls of the storage ring and a tagger shielding box. Therefore, the photon count based on the tagger was reduced by 4.2%. The reduced number of photons was divided into the total-energy bins, following the differential cross section of laser Compton scattering [11]:

$$\frac{d\sigma}{dk} = \frac{2\pi r_e^2 a}{k_{\max}}\left(\frac{[1-\rho(1+a)]^2}{[1-\rho(1-a)]^2} + \frac{\rho^2(1-a)^2}{1-\rho(1-a)} + 1\right), \quad (1)$$

where $\rho = \frac{k}{k_{\max}}$ and $a = \frac{m_e^2}{m_e^2+4E_e k_{\mathrm{inj}}}$ by using a photon beam energy k, its maximum value $k_{\max}$, the injected laser energy k_{inj}, the electron storage ring energy E_e, and the electron mass m_e. The constant r_e denotes the classical electron radius. A digitization of the tagger energy measurement by using finite-size scintillating fibers slightly influences the actual signal counts in the individual energy bins, whose boundaries do not match with those of fibers. The number of beam photons in each bin was corrected at a few percent level on the basis of a toy MC simulation. The incident photon counts on the target were finally obtained by multiplying with the transmission rate of the photon beam as described in Sec. II. The transmission rate was further modified by an energy-dependent factor coming from a beam path shift against a collimator (see Eq. (1) of Ref. [5]).

The systematic uncertainties of measured differential cross sections were estimated in the same way as those in Ref. [5] for individual kinematical bins by taking into account the following sources: uncertainties for the energy-dependent transmission (2.8−4.1%), acceptance variation due to observed photon beam position shifts (0.1−6.0%), variation of acceptance-corrected yields depending on the χ^2 probability cut in the kinematic fit (0.6−7.8%), and the accuracy of the target thickness (1.3%). In addition, uncertainties for the extracted signal counts were evaluated by changing the functional forms in the fits to the $\pi^0\gamma$-invariant-mass distributions. In one case, the resolution parameter of a Voigt function to reproduce the signal shape was left free, resulting in the

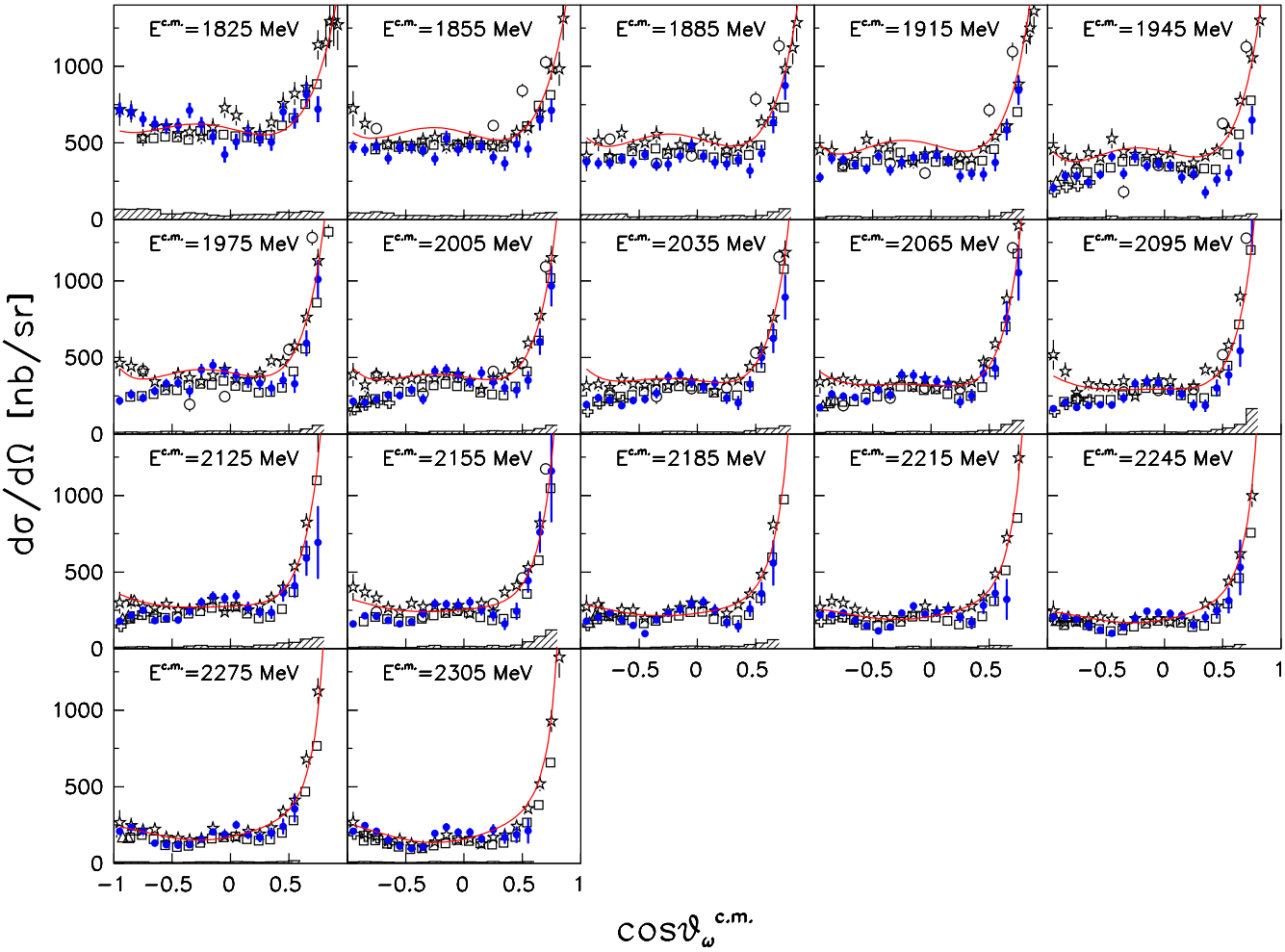

FIG. 2. Differential cross sections of the reaction $\gamma p \to \omega p$. The BGOegg results are shown by solid blue circles with statistical uncertainties. The histograms indicate systematic uncertainties. The open squares, open crosses, and open triangles come from other experimental results by the CLAS [12], LEPS [13], and LEPS-NTPC [14] Collaborations, respectively. The open circles and open stars are two independent results from Refs. [15,16], respectively, by the CBELSA/TAPS Collaboration. The overlaid lines represent the existing results of a partial-wave analysis by the Bonn-Gatchina group [17,18].

systematic uncertainties of 0.0−6.9%. In another case, an alternative background shape was adopted by using a second-order polynomial function instead of a template spectrum, giving the uncertainties of 0.1−6.4%. Finally, overall systematic uncertainties were estimated in the range of 4.0−11.7% by taking the square roots of quadratic sums.

The measured differential cross sections $d\sigma/d\Omega$ are shown by solid blue circles in Fig. 2. The statistical and systematic uncertainties are indicated by vertical bars and hatched histograms, respectively. For comparison with the existing experimental data, the results from the CLAS [12], LEPS [13,14], and CBELSA/TAPS [15,16] Collaborations were simultaneously plotted with open symbols. Because the energy-binning method is quite different among the BGOegg and those experiments, the data to be plotted were chosen by requiring the average values of the $E^{\text{c.m.}}$ bins to be the closest to the present analysis.

The BGOegg results are obtained in a wide angular range, including the most-backward acceptance, for the photon beam energies of $1.3 < E_\gamma < 2.4$ GeV. They have energy and polar angle dependence similar to that from the other experiments. In some kinematical regions, there are discrepancies in magnitude compared with the CLAS results, which have precise cross-section values in $E^{\text{c.m.}}$ bins of 10 MeV. In contrast to the CLAS measurement, which is less sensitive in the most-backward region, the two previous LEPS measurements, obtained at extremely backward angles, are consistent with the present results. These data have been measured in E_γ bins of 100 and 125 MeV for the range above 1.5 GeV. The two results from the CBELSA/TAPS experiment have been obtained in E_γ bins of 50 MeV. In Ref. [15], the differential cross sections were measured up to $E_\gamma = 2$ GeV, using less precise angular bins for backward ω emission. By contrast, the analysis in Ref. [16] adopted a $\cos\theta_\omega^{\text{c.m.}}$ bin size of 0.1 for the range of $E_\gamma < 2.5$ GeV, while the statistical uncertainties were comparable to or slightly larger than those in Ref. [15].

In Fig. 2, the experimental data are compared with a theoretical calculation by using an existing partial-wave analysis (PWA) framework by the Bonn-Gatchina group [17,18]. The PWA curves generally reproduce the forward rise of the

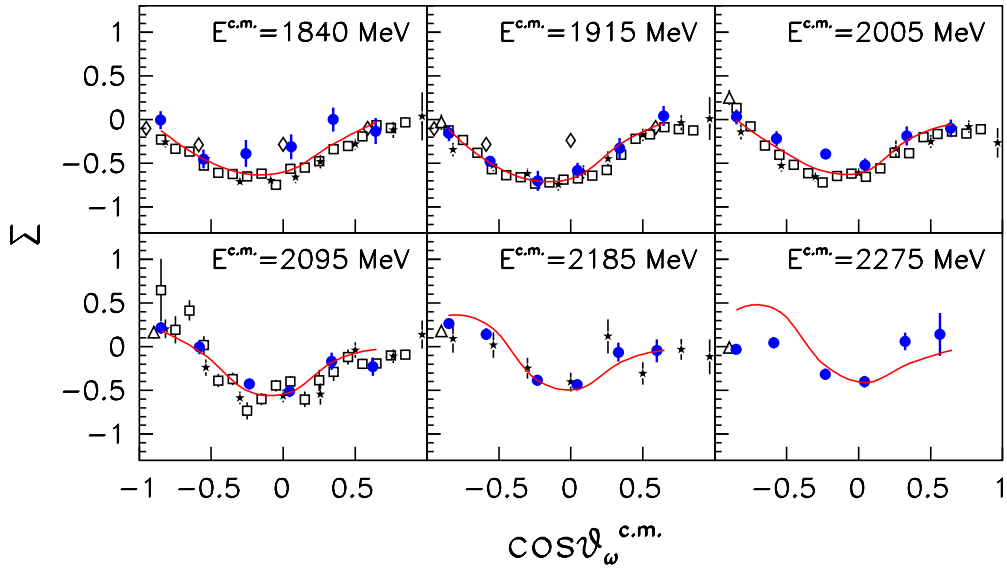

FIG. 3. Photon beam asymmetries of the reaction $\gamma p \to \omega p$. The BGOegg results are shown by solid blue circles with statistical uncertainties. The open diamonds, open triangles, open squares, and solid stars come from other experimental results by the GRAAL [19], LEPS-NTPC [14], CLAS [20], and CLAS-FROST [18] Collaborations, respectively. The overlaid lines represent the existing results of a partial-wave analysis by the Bonn-Gatchina group [17,18].

differential cross sections due to t-channel contributions, but the data points at intermediate and backward angles are not well described by them. This must come from difficulties of PWA for vector mesons and the differences between the existing experimental data.

B. Photon beam asymmetry

The photon beam asymmetry Σ is defined by the degree of skewness from an isotropic distribution of azimuthal ω-emission angles ϕ relative to the linear-polarization vector of the photon beam. The Σ was evaluated from a fit of $A(1 - P_\gamma \Sigma \cos 2\phi)$ to the measured ϕ distribution. Here A and P_γ denote a free parameter and the polarization of the photon beam, respectively. The ϕ dependence of ω-photoproduction yields was plotted in eight azimuthal-angle bins without any acceptance correction because of the symmetric geometry of the detectors. The signal yields were derived in the same way as the differential cross-section measurement except for the restriction of the proton detection area: for a proton detected at the DC, the distance of the hit point from the photon beam axis was required to be less than 600 mm to avoid artificial asymmetry due to the hexagonal shape of the DC. The photon beam asymmetries were obtained in six bins for both $-1 < \cos\theta_\omega^{\mathrm{c.m.}} < 0.8$ (a bin size of 0.3) and $1810 < E^{\mathrm{c.m.}} < 2320$ MeV (a 60-MeV bin for the lowest energies and 90-MeV bins for the remaining range).

In the measurement of photon beam asymmetries, systematic uncertainties may arise from unexpected small asymmetries of the detector geometry and ambiguities of the measured photon beam polarization. We have collected data with two linear-polarization directions, which are aligned vertically or horizontally in the laboratory frame. The influence of a possible detector asymmetry was examined by measuring the photon beam asymmetries independently with those two data sets. This source finally dominates the overall systematic uncertainties. The ambiguities of polarization direction and degree occur for the measurement of the injected laser light, whose polarization transfers to the photon beam. Such measurement uncertainties were evaluated to be relatively small. Moreover, additional uncertainties come from analysis procedures, including the background function variation in the $\pi^0\gamma$-invariant-mass fit and the azimuthal angle binning in the Σ extraction fit. They are comparable to or less than the uncertainties due to the small detector asymmetry measured using the two polarization data as mentioned above. In total, systematic uncertainties were estimated by the square root of the quadratic sum of the above estimates, resulting in the values of 0.014–0.064 for Σ. Forward-angle bins show larger uncertainties.

The photon beam asymmetries Σ obtained from the present analysis are shown by solid blue circles in Fig. 3. The measured data points are plotted at the mean $\cos\theta_\omega^{\mathrm{c.m.}}$ values of event entries in individual polar angle bins. In Fig. 3, other experimental results from the GRAAL [19], LEPS [14], and CLAS [18,20] Collaborations are overlaid with different symbols. These results have been provided in finer energy bins: 12–14 MeV for the data points from Ref. [20] and 40–60 MeV for the others. They are plotted in the panel whose central $E^{\mathrm{c.m.}}$ value is nearest to the energy bin of each measurement.

The present results by the BGOegg experiment statistically agree with the other experimental results. Precise Σ values in a wide angular range were obtained for the first time above a total energy of about 2.1 GeV. Although the LEPS results exist up to $E^{\mathrm{c.m.}} \approx 2.3$ GeV, they are limited to the extremely backward region corresponding to $\cos\theta_\omega^{\mathrm{c.m.}} < -0.8$. The GRAAL and CLAS experiments provide data in

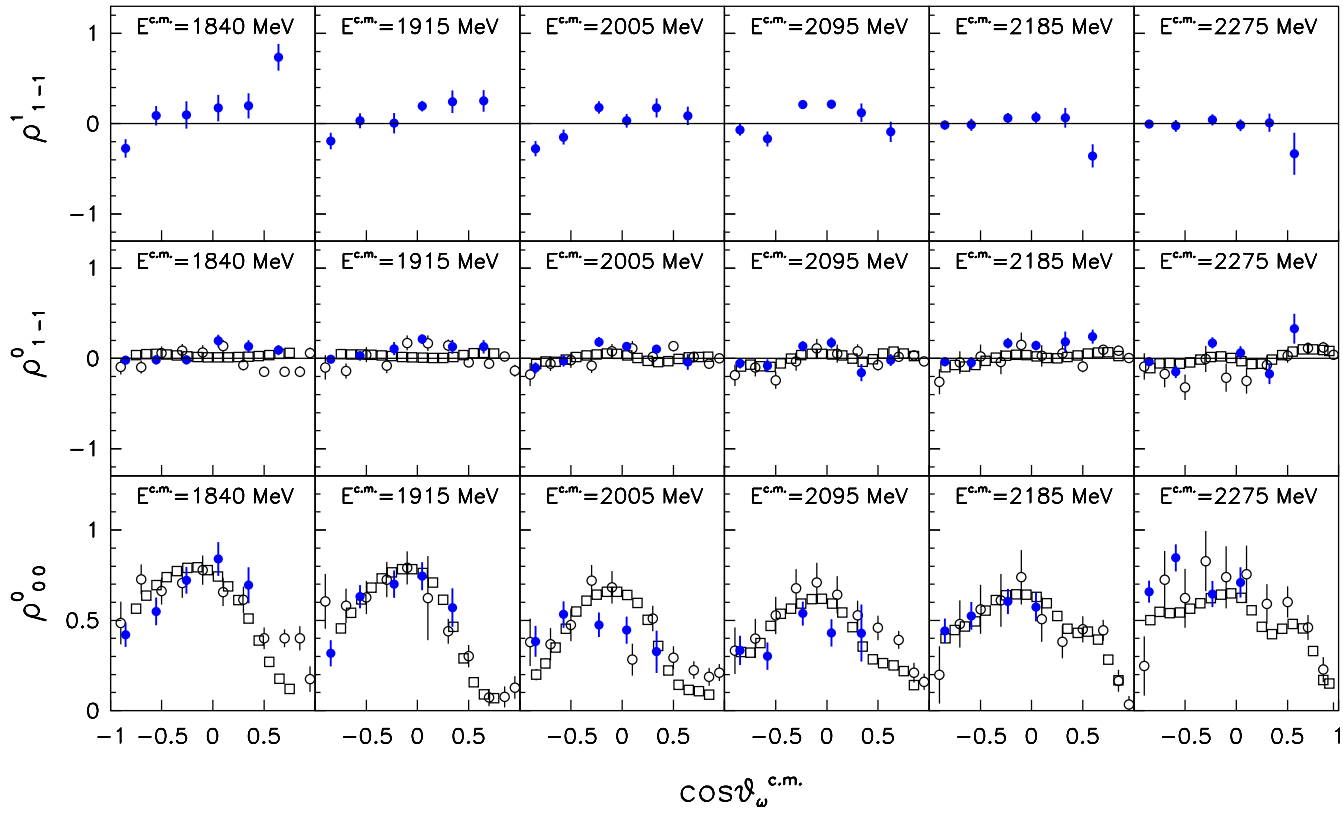

FIG. 4. Spin density matrix elements ρ^1_{1-1} (upper row), ρ^0_{1-1} (middle row), and ρ^0_{00} (lower row) of the reaction $\gamma p \to \omega p \to \pi^0 \gamma p$. The BGOegg results are shown by solid blue circles with statistical uncertainties. The open squares and open circles come from other experimental results by the CLAS [12] and CBELSA/TAPS [16] Collaborations, respectively.

a wide angular range but for total energies $E^{\text{c.m.}} \lesssim 1940$ and 2100 MeV, respectively. The recent CLAS measurement with a frozen-spin target has extended the total energy range up to 2196 MeV, but with larger statistical uncertainties at the highest energies. The solid curves in Fig. 3 show the existing PWA results calculated by the Bonn-Gatchina group [17,18]. The calculation reproduces the present results except for the highest-energy bin.

C. Spin density matrix elements

In photoproduction of a vector meson like ω, its decay angular distribution arising from the meson polarization state is influenced by helicity amplitudes. Therefore, we have additionally measured decay asymmetries or spin density matrix elements, which are sensitive to the spin information of s-channel N^* resonances and the ratio of s-, u-, and t-channel contributions. It is also important to evaluate the spin density matrix element ρ^0_{00}, which represents the unpolarized decay asymmetry in the polar angle direction, for the measurement of the geometrical acceptance factors to derive differential cross sections, as described in Sec. III C. The correct kinematical dependence can be obtained through iterative feedback for the MC simulation sample.

For ω photoproduction with a linearly polarized photon beam, the $\pi^0\gamma$-decay angular distribution $W^{\pi^0\gamma}(\Omega_\pi, \Psi)$ is expressed in the following forms after the integration over azimuthal and polar angles [21]:

$$W^{\pi^0\gamma}(\Theta) = \frac{3}{8}\left[1 + \cos^2\Theta + \rho^0_{00}(1 - 3\cos^2\Theta)\right], \quad (2)$$

$$W^{\pi^0\gamma}(\Phi, \Psi) = \frac{1}{2\pi}\left[1 - \Sigma_\Phi^{\pi^0\gamma}\cos 2\Phi - P_\gamma \Sigma_b^{\pi^0\gamma}\cos 2\Psi + P_\gamma \Sigma_d^{\pi^0\gamma}\cos 2(\Phi - \Psi)\right], \quad (3)$$

where Ω_π, Θ, and Φ denote the solid, polar, and azimuthal angles of π^0 in the ω rest frame, respectively. Here Φ is defined with respect to the reaction plane. Ψ is the angle between the linear-polarization vector and the reaction plane. In Eq. (2), the polar angle distribution of π^0 mesons is characterized by the spin density matrix element ρ^0_{00}. On the other hand, the azimuthal angle distribution is governed by unpolarized and polarized decay asymmetries $\Sigma_\Phi^{\pi^0\gamma}$ and $\Sigma_d^{\pi^0\gamma}$, which are expressed as $-\rho^0_{1-1}$ and $-\rho^1_{1-1}$, respectively, by spin density matrix elements. The polarized decay asymmetry becomes weaker proportionally to the linear-polarization degree P_γ of a photon beam. $\Sigma_b^{\pi^0\gamma}$ indicates the photon beam asymmetry of azimuthal ω-emission angles as described in Sec. IV B. In this section, we have extracted ρ^0_{00}, ρ^0_{1-1}, and ρ^1_{1-1} by fitting Eqs. (2) and (3) with integration over their unrelated angle variables.

The measured spin density matrix elements are shown by solid blue circles in Fig. 4. These matrix elements have been derived in the Adair frame, which is defined in the ω rest frame but whose z axis is taken along the incident photon beam in the center-of-mass frame [22]. In all the measurements, the total energies and polar angles were binned in the same way as for the photon beam asymmetries. The spin density matrix element ρ^1_{1-1} was obtained from the azimuthal angular dependence of π^0 in the $\omega \to \pi^0\gamma$ decay with respect to the linear-polarization vector of the photon beam. In this procedure, no acceptance correction was made under the assumption of detector symmetry. In contrast, the geometrical acceptance factors were taken into account for ρ^0_{1-1} and ρ^0_{00}, which were measured from the azimuthal and polar angular distributions of π^0 in the ω decay with respect to the reaction plane and the z axis, respectively. The correction by the photon beam polarization P_γ was done for ρ^1_{1-1}, but not for ρ^0_{1-1} and ρ^0_{00}.

The spin density matrix element ρ^1_{1-1} corresponds to the pion asymmetry Σ_π measured by the CBELSA/TAPS Collaboration [23]. We obtained small absolute values for this polarized decay asymmetry, as already seen in the Σ_π measurement. Our measurement provides new data with good precision for the photon beam energies greater than 1.7 GeV ($E^{\rm c.m.} = 2018$ MeV). The systematic uncertainties for ρ^1_{1-1} were estimated by taking into account the same sources as in the photon beam asymmetry measurement. The estimated uncertainties vary in the range of 0.02–0.07, where the lower-energy region gives a larger value.

The unpolarized elements ρ^0_{1-1} and ρ^0_{00} were measured by the CLAS [12] and CBELSA/TAPS [16] Collaborations before the present analysis. In Fig. 4, these values are plotted with the BGOegg results on the panel whose mean energy is closest to their measured bin. Our measurement shows that the $E^{\rm c.m.}$ and $\cos\theta^{\rm c.m.}_\omega$ dependence is close to the other experimental results. As the sources of systematic uncertainties for these spin density matrix elements, we consider their possible variation due to different angular binning in the azimuthal or polar direction as well as possible changes of extracted ω yields depending on the use of different background functions. Finally, the systematic uncertainties were estimated to be 0.01–0.03 and 0.01–0.04 for ρ^0_{1-1} and ρ^0_{00}, respectively.

V. DISCUSSIONS

In comparison with the case of π^0 photoproduction, there are difficulties in the identification of nucleon resonances from ω photoproduction because its vector nature has a spin of 1 and the number of available data is limited. The Bonn-Gatchina PWA has suggested the importance of the $N(1720)3/2^+$ resonance near threshold based on the data from CBELSA/TAPS [16], CLAS [20], CLAS-FROST [18], etc. However, other analyses have claimed major contributions from $N(1680)5/2^+$, $N(1700)3/2^-$, or $N(1710)1/2^+$ [20,24,25] instead of $N(1720)3/2^+$. At higher energies, resonance contributions from $1/2^-$, $1/2^+$, $3/2^+$, $3/2^-$, $5/2^+$, or $7/2^-$ partial waves have been suggested in the mass range of 1.9–2.2 GeV with variations depending on the analyses [16,18,25]. To get rid of this controversial situation, further data are definitely needed, including new information on spin observables. For example, the CLAS-FROST Collaboration has recently conducted a new PWA based on their double-polarization experiments [26]. Furthermore, our measurements of photon beam asymmetries and spin density matrix elements ρ^1_{1-1} provide first-time results with high accuracy over wide polar angles and higher energies exceeding $E^{\rm c.m.} \approx 2$ GeV. A simultaneous derivation of the beam and decay asymmetries with differential cross sections and other spin density matrix elements will be helpful to increase the experimental database of observables for ω photoproduction.

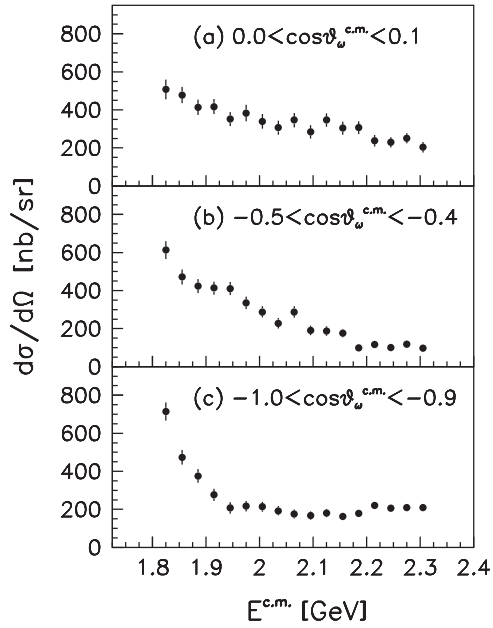

FIG. 5. Total energy dependence of the measured differential cross sections for three $\cos\theta^{\rm c.m.}_\omega$ bins. The BGOegg results are shown with statistical uncertainties only.

As shown in Fig. 2, differential cross sections measured by the present analysis are close to other experimental results except that the CBELSA/TAPS experiments provide higher values at backward angles. Although the most-forward acceptance is lacking, the forward rise due to t-channel exchange contributions is clearly seen. There is a broad bump structure at intermediate polar angles. The present results give slightly larger values compared with the CLAS measurement in this polar angle region, and the reason for this discrepancy is not yet known. Note that the differential cross sections of π^0 photoproduction are consistent between the two experiments over a wide angular range, as seen in Ref. [5]. Figures 5(a) and 5(b) show that the differential cross sections at intermediate and backward angles decrease as the total energy increases. On the other hand, those at extremely backward angles stop decreasing above $E^{\rm c.m.} \approx 1.95$ GeV, as recognized from Fig. 5(c). Although backward rises of the differential cross sections are seen at higher energies in Fig. 2, u-channel contributions are expected to be relatively small as discussed in Refs. [14,25]. In Fig. 5(c), the clear bump structure as seen in Ref. [14] is not observed, but multiple s-channel resonances with high spins may possibly contribute at backward angles, as mentioned in the beginning of this section.

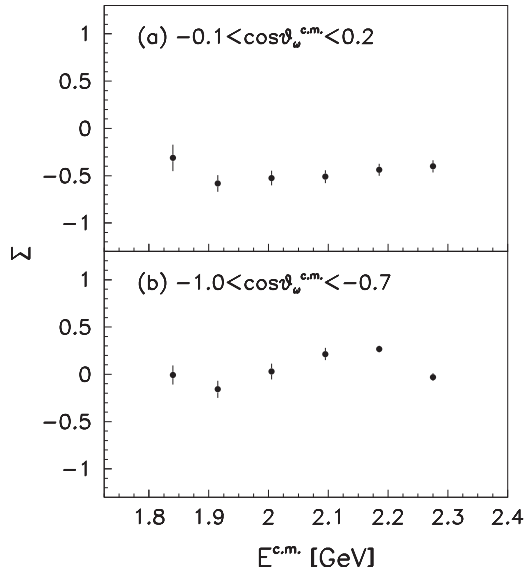

FIG. 6. Total energy dependence of the measured photon beam asymmetries for two $\cos\theta_{\omega}^{\mathrm{c.m.}}$ bins. The BGOegg results are shown with statistical uncertainties only.

The measured photon beam asymmetries show large absolute values at intermediate polar angles, in the same way as other experimental results (see Fig. 3). This must be caused by the interference between t-channel exchange processes and s-channel resonance contributions, as discussed in Refs. [18–20,23]. On the other hand, the asymmetries are close to zero in the forward region where a dominance of t-channel contributions is expected. Our results generally agree with the precise values from the CLAS Collaboration [20]. In the low-energy bins ($E^{\mathrm{c.m.}} = 1840$ and 1915 MeV), there are discrepancies between the CLAS and GRAAL [19] results. Our Σ values are closer to the CLAS results in the second-lowest-energy bin, while it is hard to clarify the consistency with either result in the lowest-energy bin due to the large statistical uncertainties of our data. Measurements in the highest-energy bin ($E^{\mathrm{c.m.}} = 2275$ MeV) provide first-time results over a wide polar angle range, as mentioned in Sec. IV B. Moreover, the present results in the second-highest-energy bin ($E^{\mathrm{c.m.}} = 2185$ MeV) improve statistical uncertainties, compared with the CLAS-FROST results [18]. Already existing solutions from the Bonn-Gatchina PWA are consistent with our results up to $E^{\mathrm{c.m.}} = 2230$ MeV, but the new data points in the highest-energy bin are not reproduced by the Bonn-Gatchina calculation, especially at backward angles, where the experimental Σ values are close to zero. Figure 6 shows the total energy dependence of Σ's measured in the present analysis for intermediate [panel (a)] and backward [panel (b)] angles. For the intermediate polar angle region, the absolute values become gradually smaller at higher energies. At the most-backward angles, the Σ values are found to have a bump structure around a total energy of 2100–2150 MeV, as discussed in Ref. [14]. Our new results should shed light on the controversial situation for high-spin states with masses above approximately $1.9\,\mathrm{GeV}/c^2$, as commented in the beginning of this section.

The polarized spin density matrix element ρ^1_{1-1} provides new information on reaction mechanisms in ω photoproduction. It becomes $+0.5$ and -0.5 in the cases of purely exchanging a pomeron and a pion in the t-channel, respectively. On the other hand, s- and u-channel contributions return $\rho^1_{1-1} = 0$. This spin density matrix element represents the azimuthal decay asymmetry of the $\omega \to \pi^0\gamma$ decay relative to the photon beam polarization direction, so that it corresponds to the pion asymmetry Σ_π measured by the CBELSA/TAPS Collaboration [23] up to $E_\gamma = 1700$ MeV. In the overlapping energy region ($1300 < E_\gamma < 1700$ MeV, or the three lower-energy bins in the upper row of Fig. 4), both BGOegg and CBELSA/TAPS results consistently show that the values of ρ^1_{1-1} or Σ_π are close to zero over a wide angular range and that they slightly increase as the ω meson is emitted at more-forward angles. Our results in the three higher-energy bins are new and indicate the dominance of s-channel resonances even at these energies. A decrease of the ρ^1_{1-1} values as a function of the total energy is also observed at forward angles.

The unpolarized spin density matrix elements ρ^0_{1-1} and ρ^0_{00} are sensitive to double and single helicity-flip amplitudes in ω photoproduction, respectively. They have been measured by the CLAS [12] and CBELSA/TAPS [16] Collaborations at the photon beam energies including the range of the BGOegg experiment, as shown in the middle and lower rows of Fig. 4. For both elements, our measurements show the values consistent with the other experimental results, although they are influenced by statistical uncertainties larger than the CLAS results. The measured ρ^0_{1-1} is close to zero for all kinematical bins and possesses small nonzero values depending on the polar angle of ω-meson emission. The ρ^0_{00} shows large values at intermediate angles, while an increase toward higher energies is seen at backward angles. The observed behaviors of the helicity-flip amplitudes surely reflect the contributions of N^* resonances.

VI. SUMMARY

We measured differential cross sections, photon beam asymmetries, and spin density matrix elements ρ^1_{1-1}, ρ^0_{1-1}, ρ^0_{00} for the reaction $\gamma p \to \omega p$, where the ω meson was detected in the $\omega \to \pi^0\gamma \to \gamma\gamma\gamma$-decay mode. A linearly polarized photon beam in the energy range of 1.3–2.4 GeV was obtained at the SPring-8 LEPS2 beamline and injected onto a 54-mm-thick LH_2 target. The three γ's in the final state were measured by a large acceptance electromagnetic calorimeter of the BGOegg experiment to identify the ω mesons in their invariant mass distribution. A signal sample was selected based on a kinematic fit, along with the information about the four-momenta of the γ's, the direction of a final-state proton detected at the BGOegg calorimeter or at the DC, and the photon beam energy measured by the tagger. Signal counts were finally evaluated by a maximum likelihood fit of a Voigt function and template background shapes.

The above observables were derived in kinematical bins of total energies and ω polar angles, covering 1810–2320 MeV and $-1 \leqslant \cos\theta_{\omega}^{\mathrm{c.m.}} \leqslant 0.8$. Our results mostly reproduce the existing data in the overlapping kinematical regions. Differential cross sections at extremely backward angles do not

decrease as the total energy increases, in contrast with the monotonic decreasing behaviors at other backward and intermediate angles. This may indicate one or more high-mass N^* resonances having high spin, which are still controversial under the current situation of ω-photoproduction analyses. We obtained photon beam asymmetries and spin density matrix elements ρ^1_{1-1} up to the total energies exceeding about 2 GeV, where the observables with a linearly polarized photon beam were previously unexplored. In the highest-energy bin, the photon beam asymmetries of backward-angle ω photoproduction deviate from the existing PWA calculation, indicating new constraints for high-spin resonances. The measured ρ^1_{1-1} values were close to zero, suggesting the dominance of s-channel resonances even at higher energies. The unpolarized spin density matrix elements ρ^0_{1-1} and ρ^0_{00} also provide spin information of resonances through helicity-flip amplitudes.

ACKNOWLEDGMENTS

The experiment was performed at the BL31LEP of SPring-8 with the approval of the Japan Synchrotron Radiation Institute (JASRI) as a contract beamline (Proposal No. BL31LEP/6101). The authors greatly acknowledge the support of the staff at SPring-8 for helping in the commissioning of the LEPS2 beamline and providing excellent experimental conditions during the data collection. We thank T. Sato, A. Sarantsev, and V. Nikonov for discussions on theoretical issues. This research was supported in part by the Ministry of Education, Culture, Sports, Science and Technology of Japan, JSPS KAKENHI Grant No. 24244022, Scientific Research on Innovative Areas Grant No. 21105003, Grant-in-Aid for Specially Promoted Research Grant No. 19002003, and the Ministry of Science and Technology of Taiwan.

[1] E. Klempt and J.-M. Richard, Rev. Mod. Phys. **82**, 1095 (2010).
[2] S. Capstick and W. Roberts, Prog. Part. Nucl. Phys. **45**, S241 (2000).
[3] V. Crede and W. Roberts, Rep. Prog. Phys. **76**, 076301 (2013).
[4] A. V. Anisovich *et al.*, Phys. Lett. B **766**, 357 (2017).
[5] N. Muramatsu *et al.*, Phys. Rev. C **100**, 055202 (2019).
[6] T. Ishikawa *et al.*, Nucl. Instrum. Methods Phys. Res., Sect. A **837**, 109 (2016).
[7] N. Muramatsu *et al.*, Nucl. Instrum. Methods Phys. Res., Sect. A **737**, 184 (2014).
[8] http://www.spring8.or.jp/en/users/operation_status/schedule/bunch_mode.
[9] M. Tanabashi *et al.* (Particle Data Group), Phys. Rev. D **98**, 030001 (2018).
[10] S. Agostinelli *et al.*, Nucl. Instrum. Methods Phys. Res., Sect. A **506**, 250 (2003); J. Allison *et al.*, IEEE Trans. Nucl. Sci. **53**, 270 (2006).
[11] A. D'Angelo *et al.*, Nucl. Instrum. Methods Phys. Res., Sect. A **455**, 1 (2000).
[12] M. Williams *et al.*, Phys. Rev. C **80**, 065208 (2009).
[13] M. Sumihama *et al.*, Phys. Rev. C **80**, 052201(R) (2009).
[14] Y. Morino *et al.*, Prog. Theor. Exp. Phys. **2015**, 013D01 (2015).
[15] F. Dietz *et al.*, Eur. Phys. J. A **51**, 6 (2015).
[16] A. Wilson *et al.*, Phys. Lett. B **749**, 407 (2015); V. Crede (private communication).
[17] A. V. Sarantsev and V. A. Nikonov (private communication).
[18] P. Roy *et al.*, Phys. Rev. C **97**, 055202 (2018).
[19] V. Vegna *et al.*, Phys. Rev. C **91**, 065207 (2015).
[20] P. Collins *et al.*, Phys. Lett. B **773**, 112 (2017).
[21] A. I. Titov and B. Kämpfer, Phys. Rev. C **78**, 038201 (2008).
[22] K. Schilling, P. Seyboth, and G. Wolf, Nucl. Phys. B **15**, 397 (1970).
[23] F. Klein *et al.*, Phys. Rev. D **78**, 117101 (2008).
[24] J. Barth *et al.*, Eur. Phys. J. A **18**, 117 (2003).
[25] M. Williams *et al.*, Phys. Rev. C **80**, 065209 (2009).
[26] P. Roy *et al.*, Phys. Rev. Lett. **122**, 162301 (2019).